Sea-Ice Reemergence in a Model Hierarchy

Mitchell Bushuk[1] and Dimitrios Giannakis[1]

Corresponding author: Mitch Bushuk, Center for Atmosphere Ocean Science, Courant Institute of Mathematical Sciences, New York University, 251 Mercer Street, New York, NY, 10012, USA. E-mail: bushuk@cims.nyu.edu

[1]Courant Institute of Mathematical Sciences, New York University, New York, New York, USA.

Lagged correlation analysis of Arctic sea-ice area reveals that spring sea-ice anomalies tend to recur the following fall, and fall anomalies tend to recur the following spring. In this work, a climate-model hierarchy is used to investigate the relative role of the atmosphere and the ocean in driving this phenomenon, termed sea-ice reemergence. Coupled data analysis of sea-ice concentration (SIC), sea-surface temperature (SST), and sea-level pressure (SLP) is performed, and families of modes that capture reemergence are constructed. In models with ocean-to-atmosphere coupling, these "reemergence families" display a pan-Arctic scale organization of SIC anomalies, related to SLP teleconnection patterns. The ocean is found to provide the key source of memory for reemergence, as an SST-based reemergence mechanism can operate as a stand-alone process, while an SLP-based mechanism cannot. Dynamical feedback from the ocean to the atmosphere is found to be essential in creating large-scale organized patterns of SIC–SLP co-variability.

1. Introduction

Satellite observations since 1979 have documented rapid changes in Arctic sea ice, spurring increased focus on Arctic prediction and predictability [eg; *Stroeve et al.*, 2014; *Tietsche et al.*, 2014; *Guemas et al.*, 2014]. A key element of this effort is the identification of physically-based mechanisms for sea-ice predictability. Sea-ice reemergence, a phenomenon in which sea-ice area anomalies tend to recur at time lags of 5–12 months, is an example of one such mechanism, originally identified by *Blanchard-Wrigglesworth et al.* [2011]. Sea-ice reemergence is observed in two main forms: (1) a spring-to-fall reemergence, related to the imprinting and summer persistence of sea-surface temperature (SST) anomalies in the seasonal ice zones, and (2) a fall-to-spring reemergence, related to winter persistence of sea-ice thickness (SIT) anomalies in the central Arctic [*Blanchard-Wrigglesworth et al.*, 2011; *Holland et al.*, 2013; *Day et al.*, 2014; *Bushuk et al.*, 2014, 2015].

The study of *Bushuk et al.* [2015] also identified an atmospheric role in spring-to-fall reemergence, relating reemerging sea-ice concentration (SIC) patterns to pan-Arctic scale sea-level pressure (SLP) teleconnection patterns. These patterns closely resemble the Arctic Dipole Anomaly [DA, *Wu et al.*, 2006] and Arctic Oscillation [AO, *Thompson and Wallace*, 1998] patterns of SLP variability. This study also corroborated earlier findings on the SST–SIC spring-to-fall reemergence mechanism, and suggested a possible SLP–SIC mechanism, in which SIC anomalies reemerge due to winter-to-winter regime persistence of large-scale atmospheric circulation patterns. *Bushuk et al.* [2015] did not quantify the relative importance and possible inter-dependence of these two mechanisms. In the present work, we explore a model hierarchy to gain insight into the relative roles of the ocean and the atmosphere in producing sea-ice reemergence. Our main finding is that the SST–SIC mechanism can exist as a stand-alone process, while the SLP–SIC mechanism cannot. Nevertheless, the atmosphere is found to a play a crucial role in setting SIC patterns of reemergence, particularly in models that have full coupling between the atmosphere and the ocean.

Sea-ice reemergence requires two elements: (1) a source of sea-ice variability to create initial sea-ice anomalies and (2) a source of memory, which allows these anomalies to reemerge at some time in the future. Reemergence has been studied in observations and comprehensive climate models, both of which involve full-physics and fully-coupled ocean, atmosphere, and sea-ice components. In this study, we analyze a hierarchy of models using the Community Climate System Model version 4 [CCSM4; *Gent et al.*, 2011], designed to probe different aspects of oceanic and atmospheric variability and memory. Summarized in Figure 1, these models consist of a fully-coupled control run, a slab ocean model (SOM) which has reduced oceanic memory, and two coordinated ocean-ice reference experiments (COREs) which have active sea-ice–ocean components forced by a specified atmosphere and lack ocean-to-atmosphere coupling. Using this model hierarchy, we perform a cross-model comparison with particular focus on: (1) the pan-Arctic, regional, and temporal aspects of sea-ice reemergence; (2) the relationship between sea-ice reemergence and SLP teleconnections; and (3) the representation of SST–SIC and SLP–SIC reemergence mechanisms.

2. Model Hierarchy and Methods

2.1. CCSM4 Model Hierarchy

We examine a hierarchy of global climate model (GCM) experiments from CCSM4, summarized in Figure 1. The fully-coupled CCSM4 successfully simulates many aspects of Arctic climate, including the SIT distribution and SIC field [*Jahn et al.*, 2012]. CCSM4 has known Arctic SLP biases, particularly a Beaufort high which is too weak and an SLP field that is generally biased low relative to reanalysis data [*de Boer et al.*, 2012]. The CCSM4 control run (b40.1850.track1.1deg.006) is 1300 years long, is forced with 1850 greenhouse gas levels, and has a grid of 1° nominal resolution for the ocean, sea-ice, and atmosphere components.

The SOM is the "CCSM4-NEWSOM", as described in *Bitz et al.* [2012]. The SOM has full atmosphere and sea-ice components, a mixed-layer ocean, and is forced with 1850 greenhouse gas levels. The mixed-layer depth, computed from an ocean general circulation model (OGCM) control run, is spatially-varying but fixed in time. The SOM also includes a "Q-flux" term, which accounts for changes to mixed-layer heat content due to ocean heat transport convergence. The Q-flux term, computed offline using the OGCM control run, is spatially-varying and has a seasonal cycle. The SOM run is 60 years long and shares the same grid as the control run.

The CORE runs have identical ice-ocean components to the control run, and are forced using the atmospheric data product developed in *Large and Yeager* [2004] and subsequently updated in *Large and Yeager* [2009]. We analyze CCSM4 ice-ocean runs that are forced with phase I [CORE-I; *Griffies et al.*, 2009] and phase II [CORE-II; *Danabasoglu et al.*, 2014] of the CORE forcing. The 950-yr CORE-I run is forced by normal year forcing (NYF) version 2 [*Large and Yeager*, 2009], which is a repeated climatological mean annual cycle of atmospheric state variables and fluxes. The CORE-II run is forced by interannnually varying forcing (IAF) version 2 [*Large and Yeager*, 2009], which is an estimate of the atmospheric state over the 60 year period from 1948–2007. Both CORE-I and CORE-II atmospheric fields are defined on a T62 grid (1.875° resolution). In order to focus on internal variability, we detrend the CORE-II data by subtracting the monthly linear trend from each month.

We also compare CCSM4 results to 35-years of SIC satellite observations from the Met Office Hadley Center Sea Ice and Sea Surface Temperature [HadISST; *Rayner et al.*, 2003] dataset. As with the CORE-II run, we detrend the HadISST data by subtracting monthly linear trends. All data is monthly averaged and the seasonal cycle is not removed. Retaining the seasonal cycle is crucial for our analysis of reemergence using nonlinear Laplacian spectral analysis (NLSA) modes, ahead.

2.2. Data Analysis Methods

In this work we utilize coupled NLSA, a unit-independent data analysis algorithm that extracts spatiotemporal modes of variability in multivariate datasets [*Bushuk et al.*, 2014, 2015]. Coupled NLSA is a multivariate extension of the original NLSA algorithm, which is a nonlinear data analysis technique designed to identify intrinsic timescales and spatiotemporal patterns in dynamical systems [*Giannakis and Majda*, 2012a, b, 2013]. Here, we follow the approach of *Bushuk et al.* [2015] and study the co-variability of SIC, SST, and SLP in the CCSM4 model hierarchy. For each model, we recover sets of temporal and spatiotemporal modes, and use these modes to investigate the representation of sea-ice reemergence. We refer the reader to *Bushuk et al.* [2015] and the supplementary text S1 for more details on the coupled NLSA methodology and implementation.

Coupled NLSA captures periodic modes, which represent the seasonal cycle, low-frequency modes, which capture interannual-to-decadal variability, and intermittent modes, which reflect the interaction of this periodic and low-frequency variability, in both space and time. Following *Bushuk et al.* [2015], reemergence mode families are constructed as the minimal set of modes able to qualitatively reproduce the reemergence signal of the raw SIC data. For each model, we identify a five-mode reemergence family, consisting of a low-frequency mode, and degenerate pairs of annual and semiannual intermittent modes.

3. Results

3.1. Sea-Ice Reemergence in CCSM4

We begin with a comparison of the regional sea-ice reemergence characteristics in the CCSM4 model runs and HadISST observations, shown in Figure 2. We assess sea-ice reemergence by computing time-lagged pattern correlations of the raw SIC anomaly field via the methodology of *Bushuk et al.* [2014, 2015]. For each initial month (from Jan–Dec) and lag (from 0–23 months), we report the time-mean pattern correlation, taken over all (month, month+lag) pairs in the SIC time series.

Over a pan-Arctic domain (0°–360° and 45°N–90°N), we find that the control and CORE-II experiments closely match the HadISST reemergence signal. Each of these displays a clear spring-to-fall reemergence, with spring SIC anomalies positively correlated with fall anomalies, despite a loss of correlation over the intervening summer months. The fall-to-spring reemergence is quite weak in each of these experiments. Note that if one performs time-lagged total area correlations via the methodology of *Blanchard-Wrigglesworth et al.* [2011], the fall-to-spring reemergence is more prominent, yet still significantly weaker than the spring-to-fall reemergence.

Consistent with earlier CCSM3 findings [*Blanchard-Wrigglesworth et al.*, 2011], the SOM spring-to-fall reemergence signal is significantly weaker than the control run. This suggests the crucial importance of a full-depth ocean in obtaining a realistic representation of spring-to-fall reemergence. Ahead, we will argue that the fall-to-spring reemergence is not as severely affected in the SOM.

The CORE-I run exhibits substantial sea-ice persistence and an unrealistically strong reemergence signal, likely due to the absence of atmospheric variability in this model. This suggests that internal ocean variability alone is insufficient to produce a realistic reemergence signal. Also, the SIC variability of CORE-I dramatically underestimates that of observations. The ratio of area-integrated variance in CORE-I vs HadISST is 0.01. As a comparison, the ratios are 0.72, 0.53, and 0.56 for the control, CORE-II, and SOM runs, respectively. This indicates that a reasonable representation of atmospheric variability is essential to producing reasonable sea-ice variability and reemergence.

Next, we examine the regional reemergence signals in the Bering (165°E–160°W and 55°N–65°N), Barents-Kara (30°E–90°E and 65°N–80°N), and Labrador (70°W–40°W and 45°N–80°N) seas. The CORE-I reemergence signal is too strong in all regions, relative to observations. The SOM reemergence signals are consistently weaker than the control run, and are slightly enhanced in the Bering Sea.

We find that the CORE-II run is a better match with observations than the control. Specifically, matching observations, CORE-II has a weak reemergence signal in the Bering Sea and Sea of Okhotsk (not shown), whereas the control has strong reemergence signals in these regions. CORE-II qualitatively agrees with observations in all regions, except the Labrador Sea/Baffin Bay region, where it has a weak reemergence signal. This weak reemergence signal in the Labrador Sea/Baffin Bay is a robust feature across all CCSM3 and CCSM4 runs that we have analyzed, likely related to the challenges of accurately modeling deep ocean convection in the Labrador sea [*Danabasoglu et al.*, 2012]. Interestingly, *Blanchard-Wrigglesworth and Bitz* [2014] note strong SIT biases in the CORE-II run. Despite these biases in SIT, the CORE-II SIC reemergence signal is very realistic.

Next, informed by the NLSA reemergence families, we investigate the temporal variability of sea-ice reemergence across these CCSM4 models. We compute time-lagged pattern correlations of the raw SIC data, both for the full timeseries, and conditional on times in which the low-frequency SIC mode (L_1^{SIC}) of each reemergence family is active. In all three models, we find that the conditional correlations display enhanced spring-to-fall and fall-to-spring reemergence (see Figure 3). This indicates substantial temporal variability in the strength of reemergence events across all three models. This also demonstrates that the low-frequency NLSA modes are effective predictors of these periods of enhanced reemergence.

In the SOM, the conditional correlations show a fall-to-spring reemergence of similar strength to the control and CORE-II models, but a significantly weaker spring-to-fall reemergence. The fall-to-spring reemergence occurs in regions of the central Arctic that are fully ice-covered during winter, where SSTs are unable to retain the memory of earlier SIC anomalies. Since the ocean does not participate in the fall-to-spring reemergence mechanism involving persistence of SIT anomalies, one would expect that the simplified ocean of the SOM would not impact the representation of this mechanism. Conversely, the spring-to-fall reemergence mechanism depends crucially on ocean heat storage below the mixed layer [*Holland et al.*, 2013]. Therefore one would expect decreased fidelity of this mechanism in the SOM. The conditional lagged correlations of Figure 3 are consistent with both of these expectations.

3.2. Reemergence Mechanisms and SLP–SIC Teleconnections

We now examine the spatiotemporal evolution of the NLSA reemergence families, with a particular focus on winter SIC–SLP teleconnections. Figure 4 shows winter means (January–March) of the reconstructed SIC, SST, and SLP fields of each reemergence family. These patterns are composites, computed over all times in which L_1^{SIC} of each family is active, in positive phase. The negative phase composites are similar, with opposite sign. Movie S1 shows the monthly evolution of these fields.

The winter SIC patterns are quite similar between the control and SOM runs, with an SIC dipole pattern between the Bering and Barents-Greenland-Iceland-Norwegian (Barents-GIN) Seas. The SIC pattern of CORE-II is dominated by anomalies in the Barents-GIN Seas, and lacks the North Atlantic–North Pacific dipole that characterizes the control and SOM. It should also be noted that despite being forced by a realistic atmosphere, the CORE-II SIC pattern differs substantially from the leading observational SIC mode, whether this mode is derived via EOF analysis [*Deser et al.*, 2000] or via NLSA

[*Bushuk et al.*, 2015]. The SST patterns of each family have opposite sign to the local SIC anomalies, and generally reflect the spring-to-fall SST–SIC reemergence mechanism (see Movie S1). One exception to this is the Barents region of the SOM, which does not display the summer imprinting of SST anomalies seen in the Bering Sea of the SOM and in the other models. A possible reason for this is the shallow depth of the Bering Sea, meaning the mixed layer ocean is a reasonable approximation to the true ocean dynamics of this region, and therefore provides a reasonable representation of the SST–SIC mechanism. Conversely, the Barents-GIN seas are deeper, and are likely poorly represented by the SOM.

The SLP patterns of each reemergence family provide a physical explanation for the inter-model differences in winter SIC. The SOM and control run have somewhat different SLP patterns, but share a key common feature: a transpolar advective pathway defined via geostrophic winds. This pathway creates communication between the North Atlantic and North Pacific basins, providing an SLP–SIC teleconnection between these disconnected regions. The geostrophic winds of these SLP patterns, and their associated surface air temperature advection, tend to create SIC anomalies of opposite sign in the Bering and Barents-GIN Seas. In contrast, the CORE-II run does not exhibit this transpolar advective pathway, and, correspondingly, does not display a North Atlantic–North Pacific teleconnection.

To examine this winter SLP–SIC interaction more precisely, we next consider the relationship between meridional wind and SIC in the Bering, GIN, and Barents-Kara Seas (see Figure 5). Using the reemergence families, we create indices for these regions based on spatial-mean meridional winds and spatial-mean SIC anomalies, and normalize these indices by the maximum standard deviation over the three regions. In regions where there is strong SLP–SIC co-variability, we expect a negative correlation between these indices, since positive meridional winds create negative SIC anomalies, and vice versa. The control run shows this negative correlation clearly in the Bering, GIN, and Barents-Kara Seas, all regions of significant SIC variability in this model. Similarly, the SOM shows negative correlations in the Bering and GIN seas, which dominate the winter SIC variability of this model, and no relationship in the Barents-Kara Seas, which have little winter SIC variability. CORE-II shows a clear negative relationship in the Barents-Kara Seas, a weak positive relationship in the GIN Seas, and a low-variance SIC signal in the Bering Sea. The SLP–SIC relationships in CORE-II are weaker than the other models, as they can explain the Barents-Kara anomalies, but not the GIN anomalies.

A necessary condition for an SIC–SLP teleconnection is a clear negative correlation between mean meridional wind and mean SIC in at least one region of both the North Atlantic and North Pacific. The control and the SOM clearly satisfy this necessary condition, but CORE-II does not. Why is this the case? A key difference between these three models is the lack of ocean-to-atmosphere coupling in CORE-II (see Figure 1). In particular, CORE-II ocean heat anomalies are unable to feedback on the atmosphere and modify the atmospheric state. These results suggest that this ocean-to-atmosphere coupling is essential in creating coherent pan-Arctic-scale co-variability of SIC and SLP.

Movie S1 shows that the reemergence families of the control and SOM display the previously mentioned SLP–SIC reemergence mechanism, due to their winter-to-winter

SLP regime persistence. This SLP–SIC mechanism is not well represented in the CORE-II run, as the SLP patterns are quite transient in space (Movie S1) and do not correlate as clearly with SIC anomalies (Figure 5). Conversely, the CORE-II and control runs display the SST–SIC reemergence mechanism, whereas this mechanism is not as robustly represented in the SOM. Given CORE-II's stronger and more realistic reemergence signal compared with the SOM, this suggests that the SST–SIC mechanism can operate as a stand-alone reemergence mechanism. In contrast, the SLP–SIC mechanism cannot operate as a stand-alone process, in the sense that it crucially depends on the full-depth dynamics and persistence of the ocean. This suggests that oceanic persistence is the key source of memory for sea-ice reemergence. However, this does not preclude an atmospheric role in reemergence. Given the observed pan-Arctic scale organization of SIC anomalies in the control and SOM, the atmosphere is the most likely driver of this variability, as oceanic variability does not provide a direct method of communication between different ocean basins. In the runs with ocean-to-atmosphere coupling, the atmosphere provides an important dynamical linkage, setting the spatial patterns of SIC reemergence.

4. Conclusions

We have assessed the representation of sea-ice reemergence and associated SST and SLP-based mechanisms in a hierarchy of CCSM4 models. The primary conclusions of this study are:

1. There is good quantitative agreement of pan-Arctic reemergence between observations, the control, and CORE-II. On regional scales, CORE-II matches the reemergence signal of observations better than the control.

2. Relative to observations, the reemergence signals of the SOM and CORE-I are too weak and too strong, respectively. The weak SOM reemergence signal indicates the crucial role of ocean heat anomalies stored below the mixed layer in providing memory for reemergence. The unrealistically strong reemergence in CORE-I indicates the necessity of atmospheric variability in providing a realistic representation of reemergence.

3. The control, CORE-II and SOM all exhibit substantial temporal variability in the strength of reemergence events. The low-frequency SIC modes of the NLSA reemergence families are effective predictors of periods of enhanced reemergence activity.

4. The SIC patterns of the reemergence families of the control and SOM runs exhibit a winter sea-ice teleconnection between the Bering and Barents-GIN Seas. The SLP patterns of the families are physically consistent with the SIC patterns, and allow communication between the North Pacific and North Atlantic sectors via a transpolar advective pathway. The CORE-II winter SIC pattern is dominated by anomalies in the Barents-GIN Seas, and does not exhibit this teleconnection. This suggests that dynamical feedback from the ocean to the atmosphere is essential in creating large-scale organized patterns of SIC–SLP co-variability.

5. The control run exhibits both the SST–SIC and the SLP–SIC reemergence mechanisms. The representation of the SST–SIC and SLP–SIC mechanism is degraded in the SOM and CORE-II runs, respectively. CORE-II has a more realistic reemergence signal than the SOM, suggesting that the SST–SIC mechanism is able to operate as a standalone mechanism. In models with ocean-to-atmosphere coupling, atmospheric variability plays a key role in reemergence, setting the spatial patterns of SIC reemergence.

In this study, we have attempted to gain insight into the coupled nature of sea-ice reemergence, by exploring models with active sea-ice components, but different physics and coupling of the atmosphere and the ocean. Because of the nonlinear, coupled dynamics of the atmosphere-ocean-ice system it is challenging to properly address notions of causality in this framework. Additional work, involving idealized model experiments and analysis of other GCMs is required to further test the conclusions presented in this study.

Acknowledgments. We thank Cecilia Bitz for assistance in running and interpreting the CCSM4 SOM experiments and for sharing data from previous SOM experiments. We thank Andy Majda for many stimulating discussions. We also thank Steve Yeager and Keith Lindsay for sharing the CCSM4 CORE-I dataset. Finally, we thank Gary Strand for preparation of the CCSM4 Control and CCSM4 CORE-II datasets. The research of D. Giannakis was supported by ONR DRI grant N00014-14-1-0150 and ONR MURI grant 25-74200-F7112. M. Bushuk is supported as a doctoral student on the first grant. The CCSM4 control and CORE-II data was downloaded from the Earth System Grid website (http://www.earthsystemgrid.org). The HadISST data was downloaded from the Met Office Hadley Centre website (http://www.metoffice.gov.uk/hadobs/hadisst/). The CORE-II forcing data was downloaded from http://data1.gfdl.noaa.gov/nomads/forms/core/COREv2.html, which is maintained by the Geophysical Fluid Dynamics Laboratory (GFDL). Data for the CORE-I and SOM runs was obtained from local disk on Yellowstone, the high-performance com-

puting cluster at the National Center for Atmospheric Research (NCAR), and is available upon request.

References

Bitz, C., K. Shell, P. Gent, D. Bailey, G. Danabasoglu, K. Armour, M. Holland, and J. Kiehl (2012), Climate sensitivity of the Community Climate System Model, Version 4, *J. Climate*, *25*(9), 3053–3070.

Blanchard-Wrigglesworth, E., and C. M. Bitz (2014), Characteristics of Arctic sea-ice thickness variability in GCMs, *J. Climate*, *27*(21), 8244–8258.

Blanchard-Wrigglesworth, E., K. C. Armour, C. M. Bitz, and E. DeWeaver (2011), Persistence and inherent predictability of Arctic sea ice in a GCM ensemble and observations, *J. Climate*, *24*, 231–250.

Bushuk, M., D. Giannakis, and A. J. Majda (2014), Reemergence mechanisms for North Pacific sea ice revealed through nonlinear Laplacian spectral analysis, *J. Climate*, *27*, 6265–6287.

Bushuk, M., D. Giannakis, and A. J. Majda (2015), Arctic sea-ice reemergence: The role of large-scale oceanic and atmospheric variability, *J. Climate*, doi:10.1175/JCLI-D-14-00354.1, in press.

Danabasoglu, G., S. C. Bates, B. P. Briegleb, S. R. Jayne, M. Jochum, W. G. Large, S. Peacock, and S. G. Yeager (2012), The CCSM4 ocean component, *J. Climate*, *25*(5), 1361–1389.

Danabasoglu, G., S. G. Yeager, D. Bailey, E. Behrens, M. Bentsen, D. Bi, A. Biastoch, C. Böning, A. Bozec, V. M. Canuto, et al. (2014), North Atlantic simulations in coordinated ocean-ice reference experiments phase II (CORE-II). Part I: mean states, *Ocean Modelling*, *73*, 76–107.

Day, J., S. Tietsche, and E. Hawkins (2014), Pan-Arctic and regional sea ice predictability: Initialization month dependence, *J. Climate*, *27*(12), 4371–4390.

de Boer, G., W. Chapman, J. E. Kay, B. Medeiros, M. D. Shupe, S. Vavrus, and J. Walsh (2012), A characterization of the present-day Arctic atmosphere in CCSM4, *J. Climate*, *25*(8), 2676–2695.

Deser, C., J. E. Walsh, and M. S. Timlin (2000), Arctic sea ice variability in the context of recent atmospheric circulation trends, *J. Climate*, *13*, 617–633.

Gent, P. R., G. Danabasoglu, L. J. Donner, M. M. Holland, E. C. Hunke, S. R. Jayne, D. M. Lawrence, R. B. Neale, P. J. Rasch, M. Vertenstein, et al. (2011), The Community Climate System Model Version 4, *J. Climate*, *24*(19), 4973–4991.

Giannakis, D., and A. J. Majda (2012a), Nonlinear Laplacian spectral analysis for time series with intermittency and low-frequency variability, *Proc. Natl. Acad. Sci.*, *109*, 2222–2227.

Giannakis, D., and A. J. Majda (2012b), Comparing low-frequency and intermittent variability in comprehensive climate models through nonlinear Laplacian spectral analysis, *Geophys. Res. Lett*, *39*, L10,710, doi:10.1029/2012GL051575.

Giannakis, D., and A. J. Majda (2013), Nonlinear Laplacian spectral analysis: Capturing intermittent and low-frequency spatiotemporal patterns in high-dimensional data, *Stat. Anal. Data Min.*, *6*(3), 180–194, doi:10.1002/sam.11171.

Griffies, S. M., A. Biastoch, C. Böning, F. Bryan, G. Danabasoglu, E. P. Chassignet, M. H. England, R. Gerdes, H. Haak, R. W. Hallberg, et al. (2009), Coordinated ocean-ice reference experiments (COREs), *Ocean Modelling*, *26*(1), 1–46.

Guemas, V., E. Blanchard-Wrigglesworth, M. Chevallier, J. J. Day, M. Déqué, F. J. Doblas-Reyes, N. Fučkar, A. Germe, E. Hawkins, S. Keeley, et al. (2014), A review on Arctic sea ice predictability and prediction on seasonal-to-decadal timescales, *Quarterly Journal of the Royal Meteorological Society*.

Holland, M. M., E. Blanchard-Wrigglesworth, J. Kay, and S. Vavrus (2013), Initial-value predictability of Antarctic sea ice in the Community Climate System Model 3, *Geophys. Res. Lett.*, *40*(10), 2121–2124.

Jahn, A., K. Sterling, M. M. Holland, J. E. Kay, J. A. Maslanik, C. M. Bitz, D. A. Bailey, J. Stroeve, E. C. Hunke, W. H. Lipscomb, et al. (2012), Late-twentieth-century simulation of Arctic sea ice and ocean properties in the CCSM4, *J. Climate*, *25*(5), 1431–1452.

Large, W., and S. Yeager (2009), The global climatology of an interannually varying air–sea flux data set, *Climate Dynamics*, *33*(2-3), 341–364.

Large, W. G., and S. G. Yeager (2004), Diurnal to decadal global forcing for ocean and sea-ice models: the data sets and flux climatologies, *Tech. Rep. TN-460+STR*, National Center for Atmospheric Research.

Rayner, N. A., D. E. Parker, E. B. Horton, C. K. Folland, L. V. Alexander, D. P. Rowell, E. C. Kent, and A. Kaplan (2003), Global analyses of sea surface temperature, sea ice, and night marine air temperature since the late nineteenth century, *J. Geophys. Res.*, *108*, 4407, doi:10.1029/2002JD002670.

Stroeve, J., L. C. Hamilton, C. M. Bitz, and E. Blanchard-Wrigglesworth (2014), Predicting September sea ice: Ensemble skill of the SEARCH sea ice outlook 2008–2013, *Geophys. Res. Lett.*, *41*(7), 2411–2418.

Thompson, D. W. J., and J. M. Wallace (1998), The Arctic oscillation signature in the wintertime geopotential height and temperature fields, *Geophys. Res. Lett*, *25*, 1297–1300, doi:10.1029/98GL00950.

Tietsche, S., J. Day, V. Guemas, W. Hurlin, S. Keeley, D. Matei, R. Msadek, M. Collins, and E. Hawkins (2014), Seasonal to interannual Arctic sea ice predictability in current global climate models, *Geophys. Res. Lett.*, *41*(3), 1035–1043.

Wu, B., J. Wang, and J. E. Walsh (2006), Dipole Anomaly in the winter Arctic atmosphere and its association with sea ice motion, *J. Climate*, *19*, 210–225, doi:10.1175/JCLI3619.1.

figure1.pdf

Figure 1. Schematic of the different CCSM4 runs analyzed in this study. Arrows indicate coupling between different components of the atmosphere–ocean–sea-ice system.

figure2.pdf

Figure 2. Time-lagged pattern correlations of SIC anomalies, computed for HadISST observations and various CCSM4 model runs, over different regions of the Arctic. All colored boxes are significant at the 95% level, based on a t test.

figure3.pdf

Figure 3. Time-lagged pattern correlations for different CCSM4 model runs, computed for the raw SIC anomaly data (left column) and conditional on the L_1^{SIC} mode of each reemergence family being active (right column). We condition on $\left|L_1^{\mathrm{SIC}}\right| > 2$ for the control run and $\left|L_1^{\mathrm{SIC}}\right| > 1.5$ for the CORE-II and SOM runs. All colored boxes are significant at the 95% level, based on a t test.

figure4.pdf

Figure 4. Winter mean (Jan–Mar) composites of SIC, SST, and SLP shown for reemergence families of the control, CORE-II, and SOM. The composites are computed over all times in which L_1^{SIC} of each family is active, in positive phase.

figure5.pdf

Figure 5. Scatterplots of standardized mean SIC vs mean meridional wind for the control, CORE-II, and SOM. These values are computed over winter months (Jan–March) in the Bering, GIN, and Barents-Kara Seas.

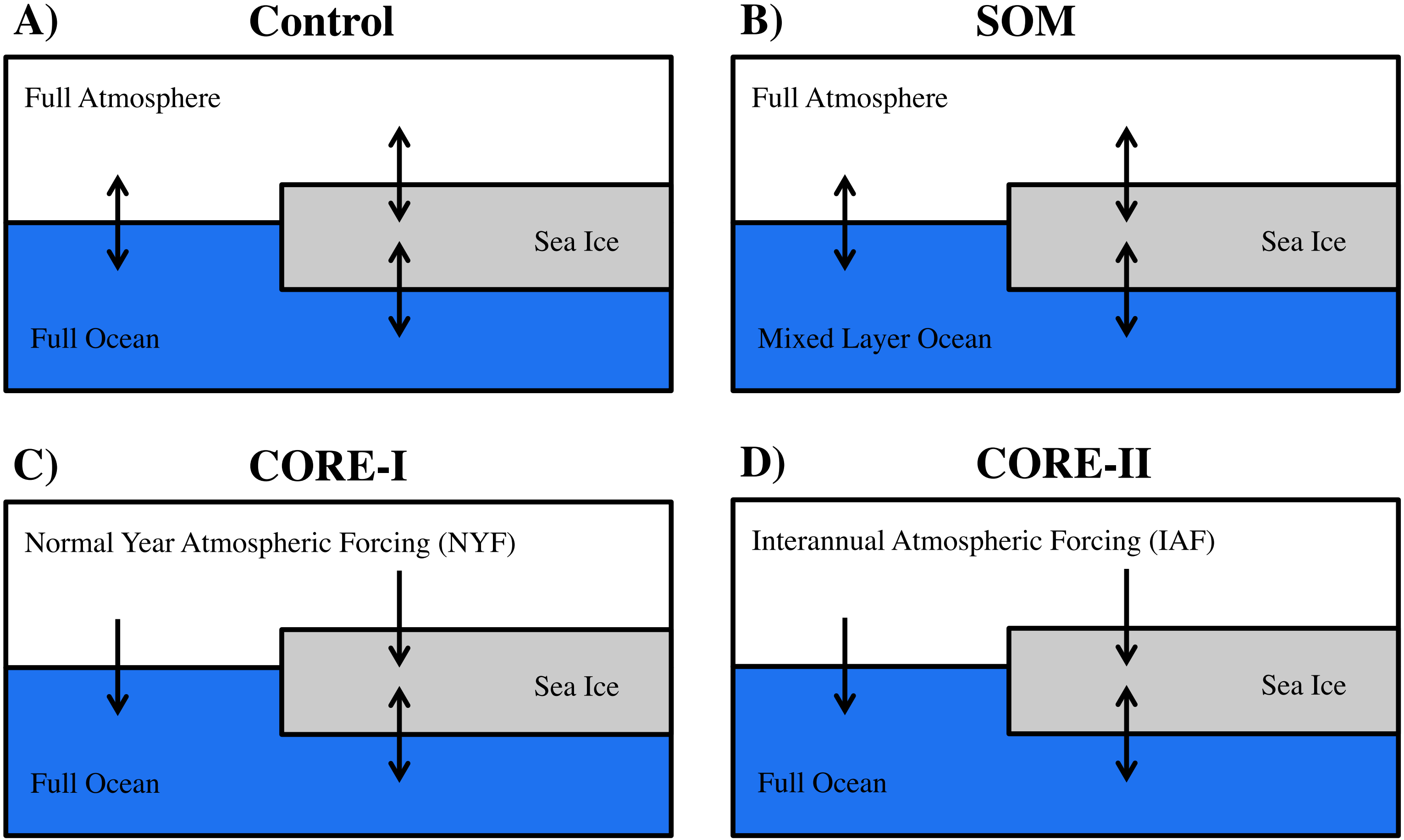
A)
Control
Full Atmosphere
Sea Ice
Full Ocean
B)
SOM
Full Atmosphere
Sea Ice
Mixed Layer Ocean
C)
CORE-I
Normal Year Atmospheric Forcing (NYF)
Sea Ice
Full Ocean
D)
CORE-II
Interannual Atmospheric Forcing (IAF)
Sea Ice
Full Ocean

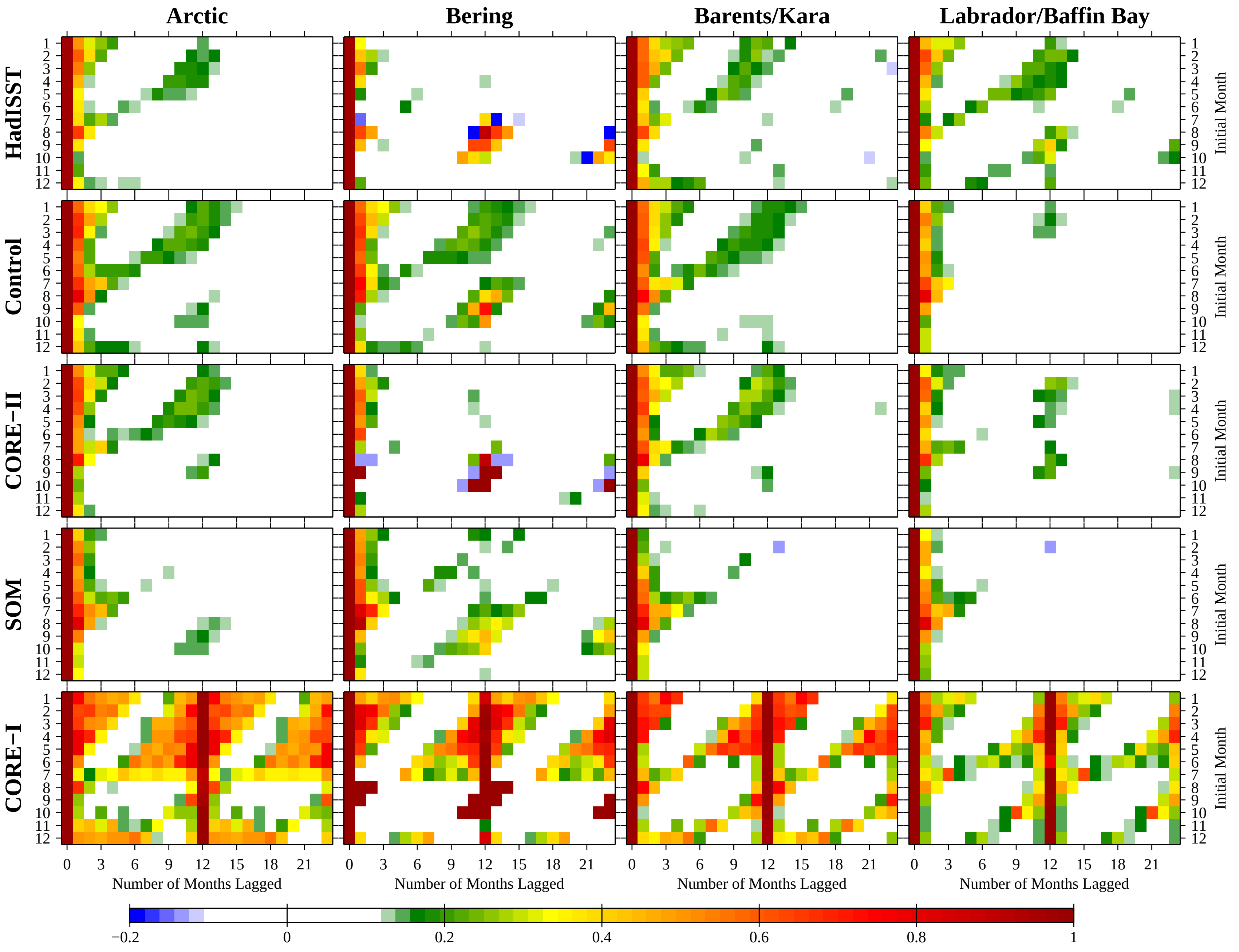

Arctic
Bering
Barents/Kara
Labrador/Baffin Bay
HadISST
Control
CORE−II
SOM
CORE−I
Initial Month
Number of Months Lagged
0 3 6 9 12 15 18 21
1 2 3 4 5 6 7 8 9 10 11 12
−0.2
0
0.2
0.4
0.6
0.8
1

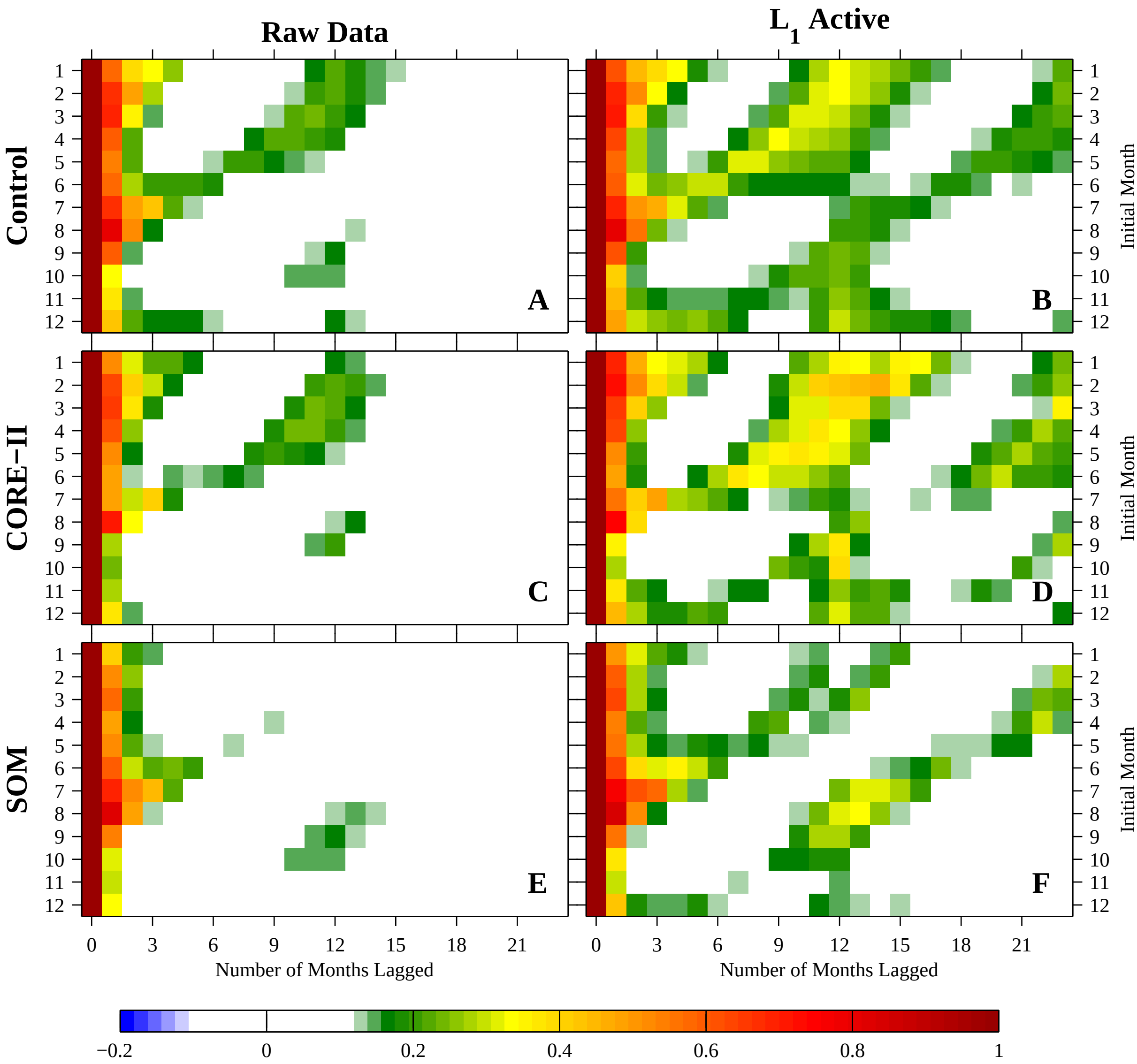

Raw Data
L$_1$ Active
Control
CORE−II
SOM
Initial Month
A
B
C
D
E
F
0 3 6 9 12 15 18 21
Number of Months Lagged
−0.2 0 0.2 0.4 0.6 0.8 1

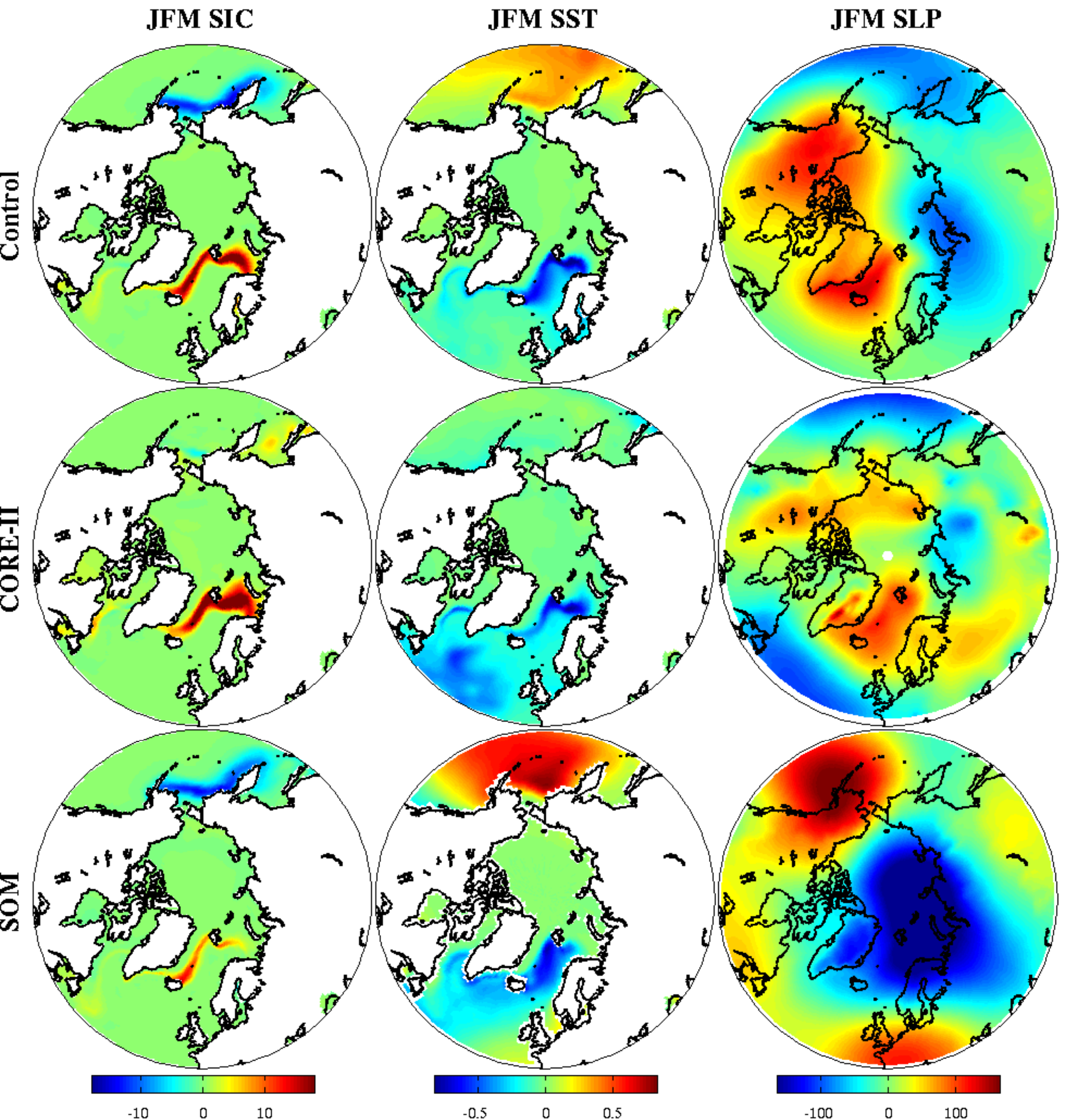

JFM SIC
JFM SST
JFM SLP
Control
CORE-II
SOM
-10
0
10
-0.5
0
0.5
-100
0
100

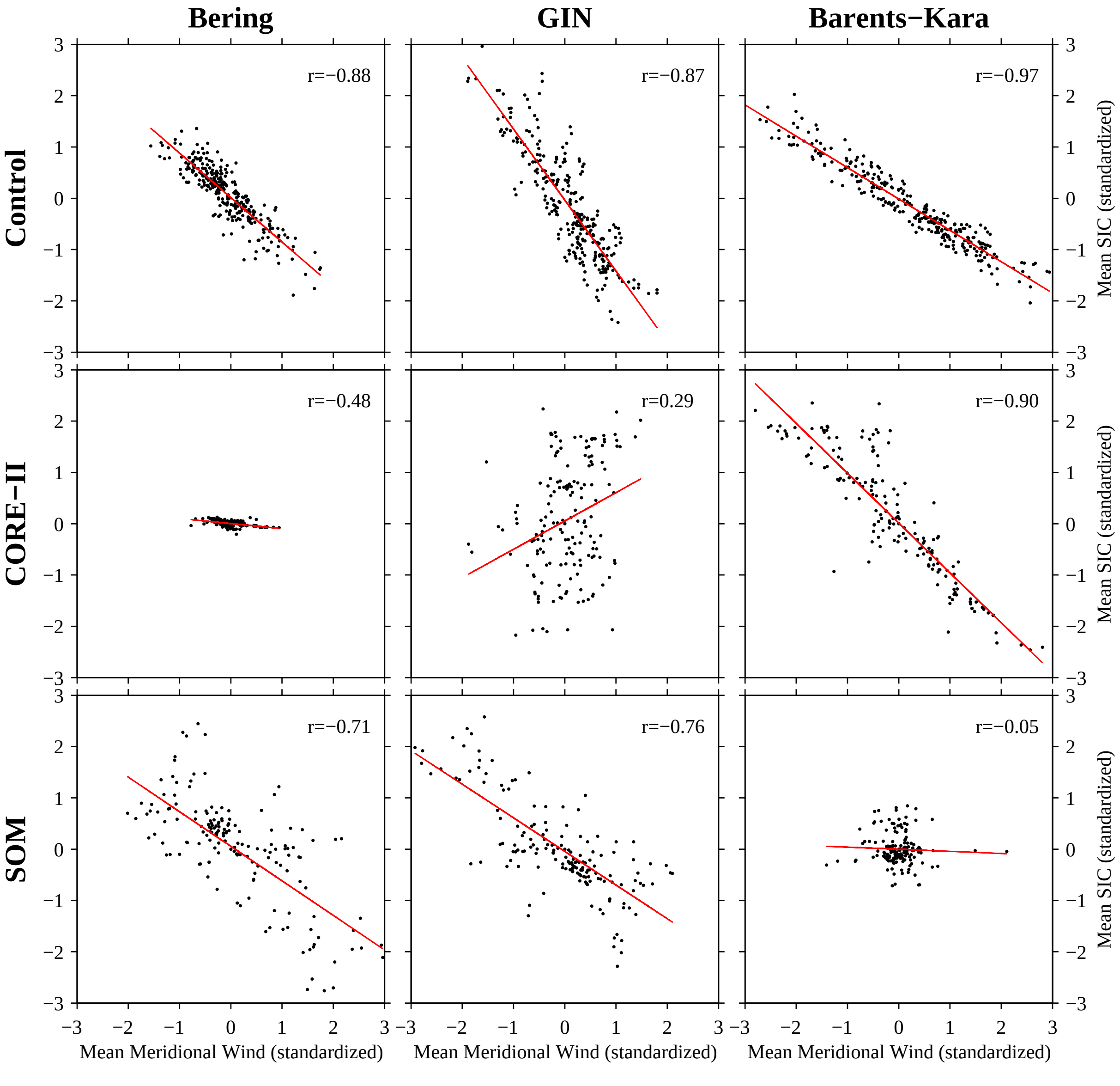
Bering
GIN
Barents−Kara
Control
CORE−II
SOM
r=−0.88
r=−0.87
r=−0.97
r=−0.48
r=0.29
r=−0.90
r=−0.71
r=−0.76
r=−0.05
Mean SIC (standardized)
Mean Meridional Wind (standardized)